Radiology

ORIGINAL RESEARCH • NEURORADIOLOGY

# Cerebellar and Brainstem Displacement Measured with DENSE MRI in Chiari Malformation Following Posterior Fossa Decompression Surgery

*Maggie S. Eppelheimer, PhD* • *Blaise Simplice Talla Nwotchouang, PhD* • *Soroush Heidari Pahlavian, PhD* • *Jack W. Barrow, MD*[1] • *Daniel L. Barrow, MD* • *Rouzbeh Amini, PhD* • *Philip A. Allen, PhD* • *Francis Loth, PhD* • *John N. Oshinski, PhD*

From the Conquer Chiari Research Center, Departments of Biomedical Engineering (M.S.E., B.S.T.N., F.L.) and Psychology (P.A.A.), University of Akron, 264 Wolf Ledges Pkwy, #211B, Akron, OH 44325; Laboratory of FMRI Technology (LOFT), USC Stevens Neuroimaging and Informatics Institute, University of Southern California, Los Angeles, Calif (S.H.P.); Mercer University School of Medicine, Savannah, Ga (J.W.B.); Departments of Neurosurgery (D.L.B.), Radiology (J.N.O.), and Imaging Sciences and Biomedical Engineering (J.N.O.), Emory University, Atlanta, Ga; and Department of Mechanical and Industrial Engineering, Department of Bioengineering, Northeastern University, Boston, Mass (R.A.). Received July 14, 2020; revision requested September 3; revision received May 2, 2021; accepted May 17. **Address correspondence to** B.S.T.N. (e-mail: *Bn23@uakron.edu*).

[1]**Current address:** Department of Radiology, University of Tennessee, Knoxville, Tenn.

Supported by the National Center for Advancing Translational Sciences of the National Institutes of Health under award number UL1TR002378, Conquer Chiari and the National Institutes of Health, National Institute of Neurological Disorders and Stroke R15 (grant 1R15NS109957-01A1).

Conflicts of interest are listed at the end of this article.

**Radiology 2021; 301:187–194 • https://doi.org/10.1148/radiol.2021203036 • Content codes: NR MR**

***Background:*** Posterior fossa decompression (PFD) surgery is a treatment for Chiari malformation type I (CMI). The goals of surgery are to reduce cerebellar tonsillar crowding and restore posterior cerebral spinal fluid flow, but regional tissue biomechanics may also change. MRI-based displacement encoding with stimulated echoes (DENSE) can be used to assess neural tissue displacement.

***Purpose:*** To assess neural tissue displacement by using DENSE MRI in participants with CMI before and after PFD surgery and examine associations between tissue displacement and symptoms.

***Materials and Methods:*** In a prospective, HIPAA-compliant study of patients with CMI, midsagittal DENSE MRI was performed before and after PFD surgery between January 2017 and June 2020. Peak tissue displacement over the cardiac cycle was quantified in the cerebellum and brainstem, averaged over each structure, and compared before and after surgery. Paired *t* tests and nonparametric Wilcoxon signed-rank tests were used to identify surgical changes in displacement, and Spearman correlations were determined between tissue displacement and presurgery symptoms.

***Results:*** Twenty-three participants were included (mean age ± standard deviation, 37 years ± 10; 19 women). Spatially averaged (mean) peak tissue displacement demonstrated reductions of 46% (79/171 μm) within the cerebellum and 22% (46/210 μm) within the brainstem after surgery ($P < .001$). Maximum peak displacement, calculated within a circular 30-mm$^2$ area, decreased by 64% (274/427 μm) in the cerebellum and 33% (100/300 μm) in the brainstem ($P < .001$). No significant associations were identified between tissue displacement and CMI symptoms ($r < .74$ and $P > .012$ for all; Bonferroni-corrected $P = .0002$).

***Conclusion:*** Neural tissue displacement was reduced after posterior fossa decompression surgery, indicating that surgical intervention changes brain tissue biomechanics. For participants with Chiari malformation type I, no relationship was identified between presurgery tissue displacement and presurgical symptoms.



*Online supplemental material is available for this article.*

Chiari malformation type I (CMI) is defined by cerebellar tonsillar descent of at least 5 mm below the foramen magnum (1–3). Patients with CMI present with a variety of neurologic symptoms, including suboccipital headaches and/or neck pain, cognitive and/or neurologic deficits, and a range of nonspecific symptoms. Patients with CMI may undergo posterior fossa decompression (PFD) surgery to reduce symptoms, restore posterior fossa cerebrospinal fluid flow, reduce tonsillar crowding, and relieve brainstem and/or cerebellar tissue compression (4,5). Although preoperative assessment includes the evaluation of tonsillar descent and other morphologic features, there are conflicting results within the literature as to whether tonsillar descent is related to CMI symptoms (1,6–8).

Patients with CMI demonstrate altered brain tissue biomechanics, characterized by increased neural tissue motion within the craniocervical region (6,9–16). Brain tissue displacement is thought to be primarily caused by changes in pressure during each heartbeat (17). Past studies have shown cerebrospinal fluid dynamics at the craniocervical region to be abnormal in participants with CMI when compared with healthy controls (18). Several studies have examined neural tissue dynamics by using phase-contrast MRI velocity measurements (6,9,10,12,13,15,16). Tissue displacement has also been quantified by integrating the phase-contrast MRI–measured velocity waveforms with respect to time over the cardiac cycle (6,9,10,13). However, phase-contrast MRI indirect measurement of

### Abbreviations

CMI = Chiari malformation type I, DENSE = displacement encoding with stimulated echoes, PFD = posterior fossa decompression


### Summary

Cerebellar and brainstem displacement measured with displacement encoding with stimulated echoes MRI in participants with Chiari malformation type I was reduced following decompression surgery.

### Key Results

- In a prospective study of 23 participants with Chiari malformation type I who underwent posterior fossa decompression surgery, displacement encoding with stimulated echoes MRI demonstrated reductions in spatially averaged peak brain tissue displacement before and after surgery of 46% (79/171 μm) within the cerebellum and 22% (46/210 μm) within the brainstem ($P < .001$).
- No significant associations between tissue displacement and presurgical symptoms were found ($r < .74$ and $P > .012$ for all; Bonferroni corrected $P = .0002$).


displacement is indirectly measured with phase-contrast MRI through the integration of velocity over the cardiac cycle and therefore may result in errors accumulating within each cardiac phase (19). Neural tissue displacement was also quantified by tracking specific anatomic points in the brainstem and the cerebellum over the cardiac cycle with use of cine MRI (11,14,20). However, these techniques are limited by the spatial resolution of the acquired image (14,20). In addition, these studies have shown inconsistent associations between tissue displacement and CMI symptoms (14,15,20).

An MRI sequence termed displacement encoding with stimulated echoes (DENSE) allows pixel-wise quantification of tissue motion over the entire brain structure by means of encoding tissue displacement into the phase of the acquired MRI signal (17,21–25). Although DENSE brain imaging has been used to evaluate displacement in healthy individuals (17,21–25), neural tissue motion has not been quantified in patients with CMI treated with surgery.

The aim of this study was to assess cerebellar and brainstem tissue motion in participants with CMI before and after PFD surgery by using DENSE MRI. Because of the altered cerebrospinal fluid dynamics and brain structure in patients with CMI, we hypothesized that neural tissue displacement will be reduced after PFD surgery. We also aimed to evaluate associations between cerebellar and brainstem tissue motion and clinical symptoms to assess the prognostic value of neural tissue displacement measurement.

## Materials and Methods

### Study Participants

This prospective study was approved by the relevant institutional review boards of the University of Akron and Emory University and compliant with the Health Insurance Portability and Accountability Act. All participants included in this study provided written informed consent. Imaging was conducted between January 2017 and June 2020; 44 consecutive patients diagnosed with CMI provided consent to participate in this study and underwent imaging (Fig 1). One surgeon (D.L.B., with 25 years of experience) recruited all participants and performed all surgeries. Patients were included if previous clinically indicated imaging showed tonsillar descent of more than 5 mm below the foramen magnum. Symptoms affected the participants such that they sought surgical treatment. Participants had experienced symptoms for more than 1 year before this study and reported that symptoms had become progressively worse since onset. Presurgical symptoms and their frequencies are presented in Table 1. Twelve participants had fewer than four symptoms, and 11 participants had five or more symptoms. Patients were excluded only if they had devices that were "MRI unsafe" or "MRI conditional" (ie, would have required monitoring or reprogramming). The surgical technique is further described in Appendix E1 (online). A previously published case-control study that investigated the differences between brain tissue displacement and strain between patients with CMI and healthy controls included pre-surgical DENSE images from 28 of the 44 consented participants used in the current study (26).

### Imaging Protocol

All imaging was performed at Emory University with a 3-T MRI scanner (Magnetom Prisma, Siemens Healthineers) by using a 20-channel head coil in combination with a table-mounted 16-channel spine coil. Peripheral pulse unit–gated cine DENSE images were acquired in a midsagittal orientation before and after PFD surgery for each participant (27). Depending on the heart rate, a total of 16–27 frames were acquired over the cardiac cycle (34 msec per frame). DENSE acquisition parameters included the following: two directions of in-plane simple motion encoding, an encoding frequency of 0.6 cycles per millimeter, 192 total spiral interleaves per image, a pixel size of 0.86–0.94 × 0.86–0.94 $mm^2$, repetition time msec/echo time msec of 17.0/2.2, and a section thickness of 8 mm. Magnitude images were used to identify brain structures, and two sets of displacement-encoded phase images (anteroposterior encoded and craniocaudal encoded) were acquired (Fig 2). Midsagittal tonsillar position and syrinx parameters were obtained in all participants by one operator (M.S.E., with 5 years of experience and trained by a board-certified neuroradiologist on brain morphometric measurements) on T1- and/or T2-weighted anatomic images and compared before and after surgery (see Appendix E1 [online]).

### DENSE Image Processing

Figure E1 (online) depicts the DENSE MRI processing method. DENSE magnitude MRI scans (Fig E1, *A* [online]) and T1- and/or T2-weighted midsagittal MRI scans obtained before and after PFD surgery were used to identify two regions of interest encompassing the brainstem and the cerebellum and manually defined by two observers (M.S.E. and B.S.T.N., with 4 years of experience and trained by a board-certified neuroradiologist on brain morphometric measurements). Tissue displacement was calculated by converting the phase information to displacement values using the encoding frequency (0.6 cycles per millimeter) at each frame of the cardiac cycle (22,24,28). DENSE images were evaluated by using an internally developed program

(DENSEpro) based on MATLAB, version R2020a (MathWorks), that allowed for selection of region of interest, unwrapping of phase images, and calculation of displacements (22). Displacement maps for the brainstem and cerebellum were obtained for each time point of the cardiac cycle (Movies 1 and 2 [online]). Only the first two thirds of the displacement waveforms were used for the calculations because T1 decay caused a reduction in the signal-to-noise ratio at the end of the cardiac cycle (19,22).

Because of the possibility of bias during the manual segmentation process, intraclass correlation was estimated for the displacement measurements between two users (M.S.E. and B.S.T.N.), both of whom were blinded to participant clinical indications at the time the measurements were conducted. No differences were found between the displacement measurements between the two users. We also identified the interrater consistency by determining the intraclass correlation (29) in the measurements between the two users. The mean difference (in micrometers) and intraclass correlation values for each parameter are shown in Table 2 ($P < .001$). MATLAB, version 2020a; SAS, version 9.4 (SAS Institute); and Microsoft Excel were used for all analyses (P.A.A. oversaw all statistical analyses).

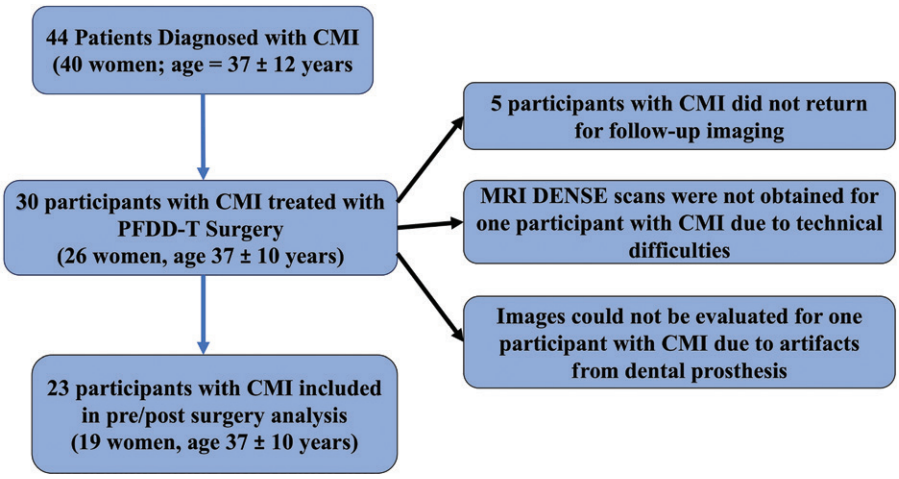


**Figure 1:** Participant flowchart. CMI = Chiari malformation type I, DENSE = displacement encoding with stimulated echoes, PFDD-T = posterior fossa decompression surgery with duraplasty and cauterization of cerebellar tonsils.

**Table 1: Frequency of Presurgical Symptoms in the 23 Evaluated Participants with Chiari Malformation Type I**

| Symptom | No. of Participants ($n$ = 23) | Condition Prevalence (%) |
|---|---|---|
| Valsalva headache | 21 | 91 |
| Subjective extremity symptoms (numbness, weakness, pain) | 20 | 87 |
| Neck pain | 11 | 48 |
| Blurry vision | 9 | 39 |
| Fatigue, lethargy | 7 | 30 |
| Hearing loss, tinnitus | 7 | 30 |
| Dizziness, vertigo | 6 | 26 |
| Headache (other) | 4 | 17 |
| Gait disturbance | 4 | 17 |
| Dysphagia | 3 | 13 |
| Memory loss | 3 | 13 |
| Chest pain | 2 | 9 |
| Anxiety, depression | 2 | 9 |
| Syncope | 2 | 7 |
| Decreased peripheral vision | 1 | 4 |
| Incontinence and/or urinary urgency | 1 | 4 |
| Arm pain | 1 | 4 |
| Shoulder pain | 1 | 4 |
| Paralysis | 1 | 4 |
| Nausea | 1 | 4 |
| Vomiting | 1 | 4 |
| Motion sickness | 1 | 4 |
| Seizure disorder | 1 | 4 |

## Calculation of Mean Displacement

Displacement magnitudes (see Appendix E1 [online]) over the cardiac cycle for the brainstem and cerebellum were calculated for all participants (Fig E1, *D* [online]). Peak tissue displacement was calculated on a pixel-by-pixel basis by using the displacement maps obtained over the cardiac cycle. The minimum tissue displacement was subtracted from maximum tissue displacement over the cardiac cycle for each pixel to obtain the peak tissue displacement (Figs 3, E1, *E* [online]) and averaged over each structure to quantify the changes in spatial mean peak displacement before and after surgery. Change in mean peak displacement was calculated as the difference between pre- and postsurgical mean peak displacement.

## Calculation of Subregion Maximum Displacement

Peak tissue displacement maps were used to quantify a subregion maximum peak tissue displacement. This analysis was undertaken to illustrate the spatial heterogeneity seen in the anatomic regions. To accomplish this, circular 30-mm$^2$ windows were passed over the peak tissue displacement maps within the cerebellum and brainstem and displacement values within those windows were averaged. The region-of-interest analysis was performed automatically in a custom-written MATLAB program. The subregions in the cerebellum and the brainstem that demonstrated the largest peak tissue displacement were identified as regions with maximum peak displacement (see Figs 4, E1, *F* [online]).

## Statistical Analysis

Paired *t* tests and nonparametric Wilcoxon signed-rank tests were used to determine differences in tonsillar herniation and neural tissue displacement before and after surgery. The Shapiro-Wilk parametric hypothesis test was used to determine nor-

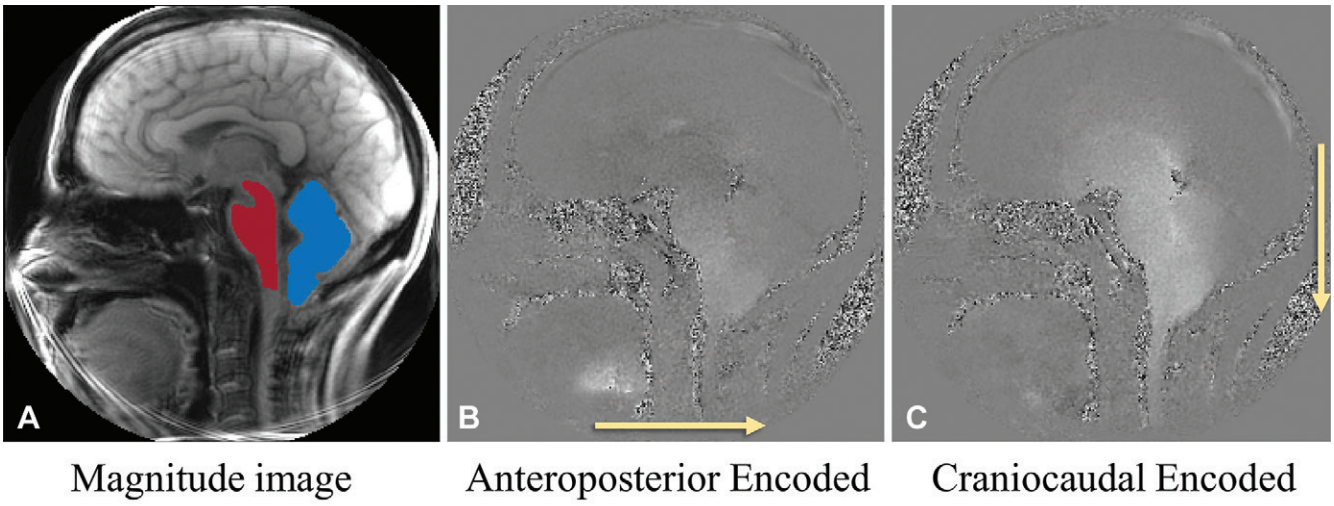


**Figure 2:** Examples of presurgical midsagittal plane displacement encoding with stimulated echoes MRI sets (each image set contains 22 frames obtained over the cardiac cycle) in participant 6, a 42-year-old woman with Chiari malformation type I. **(A)** Magnitude reconstruction (from cardiac frame 1/22) shows brainstem (red) and cerebellar mask (blue). **(B)** Phase image (from cardiac frame 15/22) with displacement encoded in the anteroposterior direction (arrow). **(C)** Phase image (from cardiac frame 15/22) with displacement encoded in the craniocaudal direction (arrow). **B** and **C** demonstrate anteroposterior and craniocaudal displacement from the frames with the peak motion. Bright pixels indicate motion to the right in **B** and in the caudal direction in **C**. No contrast agent was used in the study.

**Table 2: Intra-user Reliability Results**

| DENSE Measurement | Mean Difference (μm) | ICC |
|---|---|---|
| Mean peak displacement | | |
| Brainstem | 0.93 | 0.99 |
| Cerebellum | 2.45 | 0.99 |
| Maximum peak displacement | | |
| Brainstem | 3.64 | 0.99 |
| Cerebellum | 6.12 | 0.99 |

Note.—All ICCs were statistically significant ($P < .001$). DENSE = displacement encoding with stimulated echoes, ICC = intraclass correlation coefficient.

mality. To control for family-wise error, statistical significance was adjusted to $P < .0083$ for group differences and $P < .0002$ for all Spearman correlations between displacement, tonsillar herniation, symptoms, and syrinx area. Independent *t* tests and Wilcoxon rank-sum tests were used to evaluate displacement differences between participants with and participants without a syrinx.

## Results

### Demographic Characteristics and Symptoms

Forty-four participants (mean age ± standard deviation, 37 years ± 12; 40 women) diagnosed with CMI were included in this study (Fig 1). Thirty of the 44 participants (mean age, 37 years ± 10; 26 women) subsequently underwent PFD surgery with duraplasty and cauterization of the cerebellar tonsils. Of the 30 participants who underwent PFD surgery, five did not return for follow-up imaging. DENSE sequences were not performed in one participant because of technical difficulties, and DENSE images from an additional participant could not be evaluated because of artifacts from a dental prosthesis. Therefore, DENSE MRI scans in 23 participants with CMI before and after PFD surgery were included in the analysis (mean age, 37 years ± 10; 19 women). Peak brainstem displacement could not be quantified in two of the 23 participants (participants 4 and 21) because of dental artifacts that distorted the image. The mean time between baseline and postsurgical MRI was 133 days ± 42 (range, 94–237 days), and the average time (±standard deviation) between surgery and postsurgical MRI was 118 days ± 38 (range, 76–198 days). Tonsillar herniation decreased by 74% (7.8/10.5 mm) after surgery (from a mean of 10 mm ± 5.4 before surgery to 2.7 mm ± 4.0 after surgery; $P < .001$). This reduction in tonsillar herniation is likely due to a combination of effects from cauterization of the tonsils during surgery and change in cerebellar orientation after surgery (30).

Participants were followed up 6–8 weeks after surgery in a standard clinical follow-up visit. Twenty-two of the 23 participants had preoperative Valsalva headaches. The headaches improved or resolved after surgery in 21 of the 22 participants. Nineteen of the 23 participants had preoperative symptoms (numbness, weakness, or pain) in one or more extremities; 14 of the 19 participants improved after surgery.

Of the 23 participants evaluated, eight had syringomyelia, in which syrinxes spanned between the C2 and T2 vertebrae before surgery. Syrinx width was decreased by 68% (2.8/4.1 mm) after surgery; the average maximum syrinx width was 4 mm ± 2 before surgery and 1 mm ± 1 after surgery. Average syrinx area was decreased from 93 $mm^2$ ± 86 before surgery to 16 $mm^2$ ± 16 after surgery (Table E1 [online]). Six participants demonstrated syrinx resolution (which was determined as a presurgical syrinx that could not be identified on the postsurgical image) or a reduction in syrinx area. Two additional participants had smaller syrinxes that did not resolve after surgery (participant 8 syrinx area increased 11 $mm^2$; participant 14 syrinx area decreased 1 $mm^2$) (Table E1 [online]).

### Mean Displacement before and after Surgery

Figure 3 shows DENSE-measured peak displacement overlaid onto magnitude images of the brain before and after surgery for participant 6; these images demonstrate a large reduction in brain tissue motion after surgery. Figure 5 shows isolated pre- and postsurgical peak displacement maps for the cerebellum and brainstem for each participant in the study. A comparison of the magnitude of the mean peak displacement indicated that cerebellar mean peak displacement was reduced by 46% (79/171 μm) after PFD surgery ($P < .001$) (see Figs 5, 6A, 6B and Table 3 for spatial means). Mean peak displacement within the brainstem was reduced by 22% (46/210 μm) after surgery ($P < .001$).

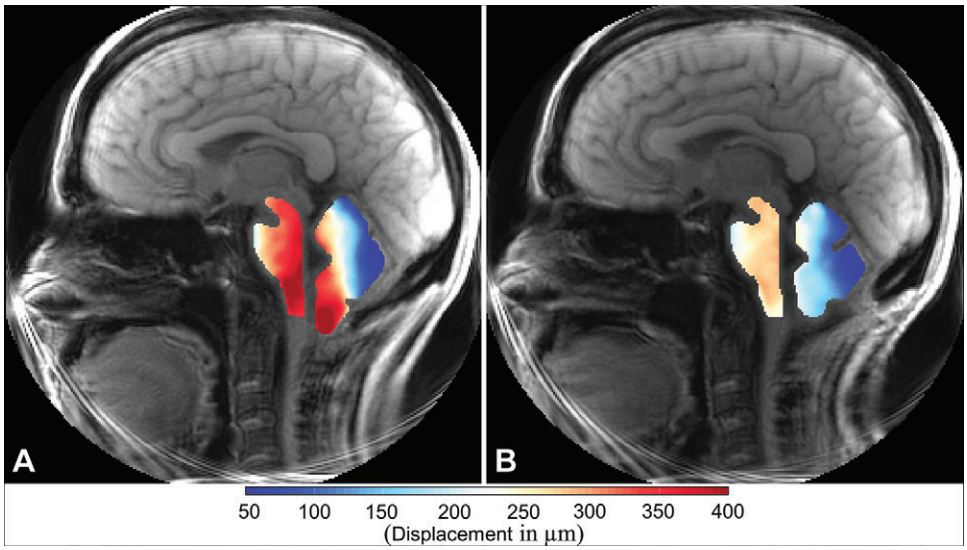


**Figure 3:** Displacement encoding with stimulated echoes magnitude images with overlays of peak displacement maps for the brainstem and cerebellum in participant 6, a 42-year-old woman with Chiari malformation type I. Images were obtained **(A)** before surgery and **(B)** after surgery. In each image, the map for the brainstem is on the left and the map for the cerebellum is on the right.

### Maximum Displacement before and after Surgery

In a circular subregion, the maximum peak displacement values within the two anatomic regions of interest (one in the brainstem and the other in the cerebellum) before and after surgery were compared (Figs 4, 6C, 6D). Cerebellar and brainstem maximum peak displacement were decreased by 64% (274/427 μm, $P < .001$) and 33% (100/300 μm, $P < .001$), respectively, after surgery.

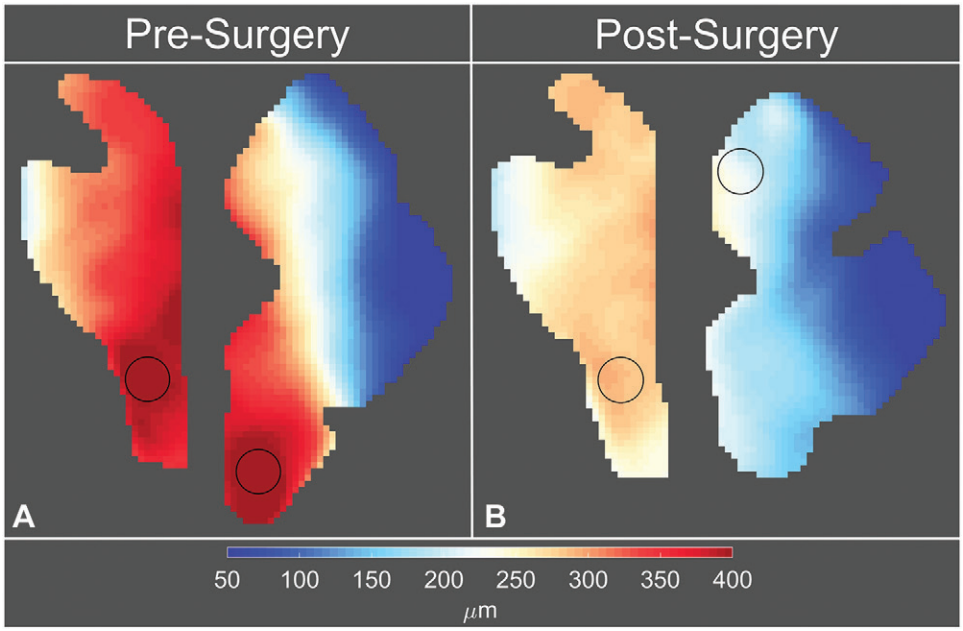


**Figure 4:** Eulerian peak displacement maps of the brainstem and cerebellum in participant 6, a 42-year-old woman with Chiari malformation type I. Images were obtained **(A)** before surgery and **(B)** after surgery. The circles on the displacement maps are the two regions of interest with maximum peak displacement.

### Associations between Presurgical Symptoms, Displacement, and Tonsillar Herniation

No presurgical symptoms demonstrated correlations with neural tissue displacement or tonsillar herniation according to our predefined cutoff that controlled for family-wise error using a Bonferroni correction for $P < .0002$ ($r < .74$ and $P > .012$ for all).

### Associations between Displacement and Syringomyelia

No significant associations were found between syrinx area and tissue displacement ($P > .036$). Presurgical cerebellar and brainstem mean peak displacement did not differ between participants with a syrinx and those without (<11 μm; $P = .929$ and $P = .757$, respectively), nor did maximum cerebellar displacement before surgery differ between participants with a syrinx and those without (< 16 μm, $P = .857$).

## Discussion

The goal of our study was to quantify the effect of posterior fossa decompression (PFD) surgery on brain tissue motion by using displacement encoding with stimulated echoes MRI, which can be used to accurately assess (31) these small regional changes on a pixel-by-pixel basis as

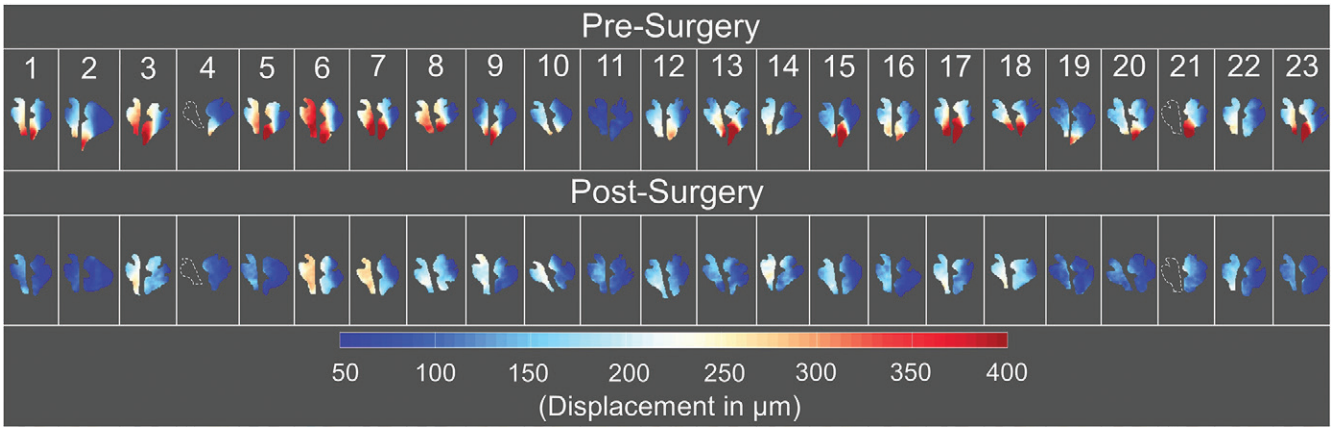


**Figure 5:** Peak displacement maps for the brainstem and cerebellum before and after surgery for all participants evaluated in this study. The brainstem peak displacement maps for participants 4 and 21 could not be acquired because of limited image quality; the outlines of the brainstem shown for these participants were acquired with sagittal T2-weighted multisection turbo spin-echo imaging (repetition time msec/echo time msec, 3500/106).

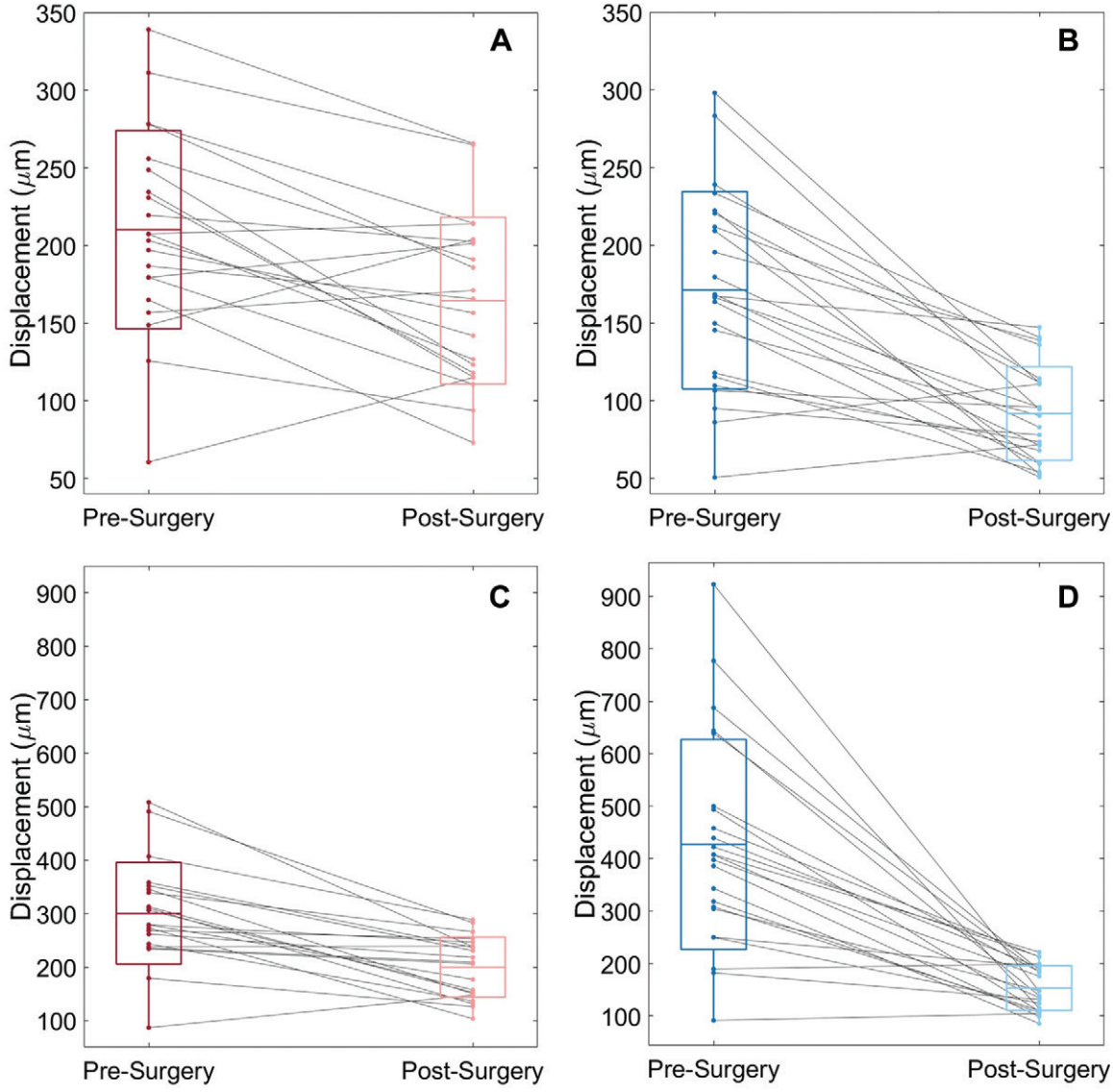


**Figure 6:** Box-and-whisker plots show mean and maximum peak displacement of **(A, C)** brainstem and **(B, D)** cerebellum for each of the 23 participants before and after surgery. Each line represents a participant. The center lines in the boxes represent the mean for each group, and the boxes represent the mean ± standard deviation. Whiskers represent the range of displacements for each group.

**Table 3: Displacements in Brainstem and Cerebellum before and after Surgery in the 23 Evaluated Participants with Chiari Malformation Type I**

| Parameter | No. of Participants | Displacement before Surgery (μm)* | Displacement after Surgery (μm)* | Mean Difference (μm) | *P* Value |
|---|---|---|---|---|---|
| Mean peak displacement | | | | | |
| Brainstem | 21 | 210 ± 64 | 164 ± 54 | 46 | <.001 |
| Cerebellum | 23 | 171 ± 63 | 92 ± 30 | 79 | <.001 |
| Maximum peak displacement | | | | | |
| Brainstem | 21 | 300 ± 95 | 200 ± 56 | 100 | <.001 |
| Cerebellum | 23 | 427 ± 200 | 153 ± 43 | 274 | <.001 |

* Data are means ± standard deviations.

well as to examine associations between tissue displacement and symptoms. Our results indicate that PFD surgery reduced displacement within the brainstem and cerebellum by 22% (46/210 μm) and 46% (79/171 μm), respectively ($P < .001$). We found postsurgical mean peak displacement within the brainstem (164 μm) and cerebellum (92 μm) to be similar to displacements found in healthy individuals, which ranged from 150 to 210 μm and from 70 to 105 μm, respectively (22,24). These similarities imply that patients with Chiari malformation type I demonstrate "normal" neural tissue motion after surgery. Although we found the change in mean peak displacement (46 μm) and maximum peak displacement (100 μm) after PDF surgery within the brainstem to be smaller than in previous phase-contrast MRI studies (150 μm) (13), this discrepancy could be due to the evaluation of a smaller region within the brainstem in the earlier studies. We found no associations between neural tissue displacement and presurgical symptoms ($r < .74$ and $P > .012$ for all; Bonferroni corrected $P = .0002$). In addition, we found a trend toward an association between presurgical tonsillar position and change in maximum peak displacement after PFD surgery within the cerebellum ($r = 0.65$, $P = .0008$).

The fundamental driving force of brain tissue motion is time-varying pressure within the cranium during the cardiac cycle. The magnitude and spatial variation of displacement depend on the magnitude of the pressure difference; the anatomic structure of the cranium, brain tissue, and cerebrospinal fluid spaces; and the biomechanical properties of the brain tissue. Therefore, changing the structure of the cranium and the anatomic structure of the cerebrospinal fluid spaces with PFD surgery is expected to alter brain motion. The spatial distribution of displacement in each of the two structures was nonuniform. This heterogeneity of displacement was evident in the larger reduction in the brainstem maximum peak displacement (100 μm) and cerebellar maximum peak displacement (274 μm) after PFD surgery as compared with the reduction in mean peak displacement for the entire brainstem (46 μm) and cerebellum (79 μm). In addition, cerebellar tonsils demonstrated less motion than the superior regions of the cerebellum and brainstem after surgery, indicating that PFD surgery has the greatest impact on the inferior cerebellar motion. The heterogeneity of the brain tissue motion will result in tissue strain because of displacement gradients within each structure (21,22,26). Tissue strain can lead to tissue damage if large enough in magnitude. Brain tissue motion distribution changes after PFD surgery indicate that surgery alters brain biomechanics and not just anatomic structure.

The change in maximum peak displacement after PDF surgery fell between the values reported by Dawes et al (median displacement, 380 μm; interquartile range, 170–920 μm) (20) and those reported by Leung et al (approximately 160–180 μm) (14). Large variation in the reported postsurgery reduction of brain tissue motion in participants with CMI might be attributed to the inherent limitation of previous tracking-based techniques that relied on a few anatomic points in the cerebellum or brainstem. Conversely, DENSE images used in our study allowed for the quantification of displacement maps over the entire brain structure within the midsagittal plane; as such, they could result in a more comprehensive picture of the tissue dynamics compared with motion-tracking methods.

Previous studies inconsistently demonstrate associations between neural tissue displacement and CMI symptoms. Both Pujol et al (15) and Leung et al (14) demonstrated larger tonsillar tissue motion or strain in participants with cough-associated (Valsalva) headaches than in participants without cough-associated headaches. However, Dawes et al (20) found no association between participants with Valsalva headaches and those with tonsillar motion. Although two previous studies found participants with larger tonsillar herniation had more severe lesions (7) or cough-associated headaches (8), two additional studies could not identify a relationship between tonsillar herniation and symptoms (1,6).

Our study had some limitations. The sample size was limited. Only 23 participants were evaluated, and the results may not be generalizable to a larger population. Postsurgical CMI symptoms were not obtained in the current study and therefore the relationship between brain tissue motion and postsurgical CMI symptoms was not evaluated. The manual segmentation of the brainstem and cerebellum is a potential source of bias. DENSE inherently requires a prospective trigger to execute a tagging pulse, and motion is measured from the point labeled by the tagging pulse. This requires some small percentage (5%) of the cardiac cycle to be missed while the sequence waits for the next trigger pulse. Because of the reduction of signal-to-noise ratio caused by a T1 decay at the end of the cardiac cycle, only the first two-thirds of the displacement waveforms were used for this study (19,22). Our implementation of the DENSE technique

did not measure displacements in the through-plane direction but examined motion only within a single midsagittal plane.

In conclusion, by using MRI-based displacement encoding with stimulated echoes, we found cerebellar and brainstem displacements to be reduced following posterior fossa decompression (PFD) surgery and surgery to have a greater impact on cerebellar motion than on brainstem motion. The results indicate that PFD surgery changes not only anatomic structures but also underlying brain tissue motion and biomechanics in a spatial heterogeneous manner. Although we found a reduction in cerebellum and brainstem motion after surgery, this reduction was not predictive of presurgical Chiari malformation type I (CMI) symptoms. Future investigations with larger sample sizes are needed to validate this lack of association between tissue displacement and presurgical symptoms and to evaluate a possible relationship between tissue displacement and surgical outcome. In addition, although displacement was not correlated with CMI symptoms, other brain biomechanical properties, such as strain, may be predictive of CMI symptoms.

**Author contributions:** Guarantors of integrity of entire study, M.S.E., B.S.T.N., F.L., J.N.O.; study concepts/study design or data acquisition or data analysis/interpretation, all authors; manuscript drafting or manuscript revision for important intellectual content, all authors; approval of final version of submitted manuscript, all authors; agrees to ensure any questions related to the work are appropriately resolved, all authors; literature research, M.S.E., B.S.T.N., P.A.A., F.L.; clinical studies, S.H.P., D.L.B., J.N.O.; experimental studies, M.S.E., B.S.T.N., S.H.P., R.A., F.L., J.N.O.; statistical analysis, M.S.E., B.S.T.N., P.A.A., F.L.; and manuscript editing, all authors

**Disclosures of Conflicts of Interest:** **M.S.E.** disclosed no relevant relationships. **B.S.T.N.** disclosed no relevant relationships. **S.H.P.** disclosed no relevant relationships. **J.W.B.** disclosed no relevant relationships. **D.L.B.** disclosed no relevant relationships. **R.A.** disclosed no relevant relationships. **P.A.A.** disclosed no relevant relationships. **F.L.** disclosed no relevant relationships. **J.N.O.** disclosed no relevant relationships.

## References

1. Milhorat TH, Chou MW, Trinidad EM, et al. Chiari I malformation redefined: clinical and radiographic findings for 364 symptomatic patients. Neurosurgery 1999;44(5):1005–1017.
2. Fischbein R, Saling JR, Marty P, et al. Patient-reported Chiari malformation type I symptoms and diagnostic experiences: a report from the national Conquer Chiari Patient Registry database. Neurol Sci 2015;36(9):1617–1624.
3. Barkovich AJ, Wippold FJ, Sherman JL, Citrin CM. Significance of cerebellar tonsillar position on MR. AJNR Am J Neuroradiol 1986;7(5):795–799.
4. Yilmaz A, Kanat A, Musluman AM, et al. When is duraplasty required in the surgical treatment of Chiari malformation type I based on tonsillar descending grading scale? World Neurosurg 2011;75(2):307–313.
5. Chavez A, Roguski M, Killeen A, Heilman C, Hwang S. Comparison of operative and non-operative outcomes based on surgical selection criteria for patients with Chiari I malformations. J Clin Neurosci 2014;21(12):2201–2206.
6. Sivaramakrishnan A, Alperin N, Surapaneni S, Lichtor T. Evaluating the effect of decompression surgery on cerebrospinal fluid flow and intracranial compliance in patients with chiari malformation with magnetic resonance imaging flow studies. Neurosurgery 2004;55(6):1344–1350; discussion 1350–1351.
7. Kavak RP, Özdemir M, Sorar M. Impact of morphological measurements on symptoms in Chiari malformation type 1. J Surg Med 2019;3(6):441–446.
8. Huang CWC, Chang YM, Brook A, Bezuidenhout AF, Bhadelia RA. Clinical utility of 2-D anatomic measurements in predicting cough-associated headache in Chiari I malformation. Neuroradiology 2020;62(5):593–599.
9. Alperin N, Loftus JR, Oliu CJ, et al. Magnetic resonance imaging measures of posterior cranial fossa morphology and cerebrospinal fluid physiology in Chiari malformation type I. Neurosurgery 2014;75(5):515–522; discussion 522.
10. Alperin N, Sivaramakrishnan A, Lichtor T. Magnetic resonance imaging-based measurements of cerebrospinal fluid and blood flow as indicators of intracranial compliance in patients with Chiari malformation. J Neurosurg 2005;103(1): 46–52.
11. Cousins J, Haughton V. Motion of the cerebellar tonsils in the foramen magnum during the cardiac cycle. AJNR Am J Neuroradiol 2009;30(8):1587–1588.
12. Hofmann E, Warmuth-Metz M, Bendszus M, Solymosi L. Phase-contrast MR imaging of the cervical CSF and spinal cord: volumetric motion analysis in patients with Chiari I malformation. AJNR Am J Neuroradiol 2000;21(1):151–158.
13. Lawrence BJ, Luciano M, Tew J, et al. Cardiac-related spinal cord tissue motion at the foramen magnum is increased in patients with type I Chiari malformation and decreases postdecompression surgery. World Neurosurg 2018;116:e298–e307.
14. Leung V, Magnussen JS, Stoodley MA, Bilston LE. Cerebellar and hindbrain motion in Chiari malformation with and without syringomyelia. J Neurosurg Spine 2016;24(4):546–555.
15. Pujol J, Roig C, Capdevila A, et al. Motion of the cerebellar tonsils in Chiari type I malformation studied by cine phase-contrast MRI. Neurology 1995;45(9):1746–1753.
16. Wolpert SM, Bhadelia RA, Bogdan AR, Cohen AR. Chiari I malformations: assessment with phase-contrast velocity MR. AJNR Am J Neuroradiol 1994;15(7):1299–1308.
17. Sloots JJ, Biessels GJ, Zwanenburg JJM. Cardiac and respiration-induced brain deformations in humans quantified with high-field MRI. Neuroimage 2020;210:116581.
18. Clarke EC, Fletcher DF, Stoodley MA, Bilston LE. Computational fluid dynamics modelling of cerebrospinal fluid pressure in Chiari malformation and syringomyelia. J Biomech 2013;46(11):1801–1809.
19. Spottiswoode BS, Zhong X, Hess AT, et al. Tracking myocardial motion from cine DENSE images using spatiotemporal phase unwrapping and temporal fitting. IEEE Trans Med Imaging 2007;26(1):15–30.
20. Dawes BH, Lloyd RA, Rogers JM, Magnussen JS, Bilston LE, Stoodley MA. Cerebellar tissue strain in Chiari malformation with headache. World Neurosurg 2019;130:e74–e81.
21. Adams AL, Kuijf HJ, Viergever MA, Luijten PR, Zwanenburg JJM. Quantifying cardiac-induced brain tissue expansion using DENSE. NMR Biomed 2019;32(2):e4050.
22. Pahlavian SH, Oshinski J, Zhong X, Loth F, Amini R. Regional quantification of brain tissue strain using displacement-encoding with stimulated echoes magnetic resonance imaging. J Biomech Eng 2018;140(8):081010.
23. Soellinger M, Rutz AK, Kozerke S, Boesiger P. 3D cine displacement-encoded MRI of pulsatile brain motion. Magn Reson Med 2009;61(1):153–162.
24. Zhong X, Meyer CH, Schlesinger DJ, et al. Tracking brain motion during the cardiac cycle using spiral cine-DENSE MRI. Med Phys 2009;36(8):3413–3419.
25. Adams AL, Viergever MA, Luijten PR, Zwanenburg JJM. Validating faster DENSE measurements of cardiac-induced brain tissue expansion as a potential tool for investigating cerebral microvascular pulsations. Neuroimage 2020;208:116466.
26. Nwotchouang BST, Eppelheimer MS, Pahlavian SH, et al. Regional brain tissue displacement and strain is elevated in subjects with Chiari malformation type I compared to healthy controls: a study using DENSE MRI. Ann Biomed Eng 2021. 10.1007/s10439-020-02695-7. Published online January 4, 2021.
27. Zhong X, Spottiswoode BS, Meyer CH, Kramer CM, Epstein FH. Imaging three-dimensional myocardial mechanics using navigator-gated volumetric spiral cine DENSE MRI. Magn Reson Med 2010;64(4):1089–1097.
28. Aletras AH, Balaban RS, Wen H. High-resolution strain analysis of the human heart with fast-DENSE. J Magn Reson 1999;140(1):41–57.
29. Houston JR, Eppelheimer MS, Pahlavian SH, et al. A morphometric assessment of type I Chiari malformation above the McRae line: a retrospective case-control study in 302 adult female subjects. J Neuroradiol 2018;45(1):23–31.
30. Eppelheimer MS, Biswas D, Braun AM, et al. Quantification of changes in brain morphology following posterior fossa decompression surgery in women treated for Chiari malformation type 1. Neuroradiology 2019;61(9):1011–1022.
31. Nwotchouang BST, Eppelheimer MS, Biswas D, et al. Accuracy of cardiac-induced brain motion measurement using displacement-encoding with stimulated echoes (DENSE) magnetic resonance imaging (MRI): A phantom study. Magn Reson Med 2021;85(3):1237–1247.